Materials Science & Engineering A 806 (2021) 140860

Contents lists available at ScienceDirect

Materials Science & Engineering A

journal homepage: http://www.elsevier.com/locate/msea

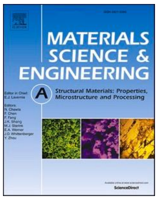

# In situ monitoring of dislocation, twinning, and detwinning modes in an extruded magnesium alloy under cyclic loading conditions

Di Xie [a], Zongyang Lyu [a], Yuan Li [a], Peter K. Liaw [a], Huck Beng Chew [b], Yang Ren [c], Yan Chen [d], Ke An [d], Yanfei Gao [a,*]

[a] *Department of Materials Science and Engineering, University of Tennessee, Knoxville, TN, 37996, USA*
[b] *Department of Aerospace Engineering, University of Illinois at Urbana-Champaign, Urbana, IL, 61801, USA*
[c] *X-ray Science Division, Argonne National Laboratory, Argonne, IL, 60439, USA*
[d] *Neutron Scattering Division, Oak Ridge National Laboratory, Oak Ridge, TN, 37831, USA*

ARTICLE INFO

*Keywords:*
Low cycle fatigue
Magnesium alloy
In situ neutron diffraction
Deformation mode transitions

ABSTRACT

This work investigates the microscopic deformation mechanisms of an extruded, precipitation-strengthened AZ80 magnesium (Mg) alloy subjected to strain-controlled low-cycle fatigue using in situ neutron diffraction measurements. Results demonstrate that the plastic deformation during cyclic loading is dominated by the alternating {10.2} extension twinning and detwinning mechanisms. The observed deformation mode is strongly texture and precipitate dependent. For the initial texture, the tested material has two major texture components which result in the occurrence of extension twinning during both compression and reverse tension in the first two cycles. The prolonged detwinning process in the following cycles is proposed to relieve the shear stress field of {00.2} grains, leading to the disappearance of twinning. The precipitation strengthening results in an increase of the critical resolved shear stress (CRSS) by ~33 MPa for the extension twinning in this AZ80 alloy. The synergistic effects of the initial texture, precipitation strengthening, and load sharing of various grain families and phases contribute to the complicated evolution of dominant deformation mechanisms, among which elevated dislocation activities are believed to be responsible for the relatively poor low-cycle-fatigue lifetime when compared to other Mg alloys.

## 1. Introduction

The accelerated maturation of magnesium alloys as structural components in the automobile and aerospace industry is driven by their unique properties of low density, high strength-to-weight ratio, and high specific stiffness [1–3]. Oftentimes, these structural components are subjected to cyclic loading conditions, and thus usually suffer sudden and catastrophic failures during the service. Therefore, failure lifetime predictions of Mg alloys through a fundamental understanding of their fatigue behavior is vital for their applications as structural alloys. Besides the standard mechanical testing and metallurgical characterizations, Mg fatigue studies have witnessed new opportunities and novel perspectives from advanced diffraction techniques at spallation neutron and synchrotron X-ray sources [4–7]. Due to their microstructural nature, advanced microscopies and diffraction facilities provide unprecedented knowledge on the deformation characteristics, such as twinning/detwinning transitions, but it still remains elusive on making a further connection between such deformation studies to the failure predictions.

Unlike face-centered-cubic (FCC) or body-centered-cubic (BCC) metal alloys such as Cu and Ni, Mg alloys are hexagonal-close-packed (HCP) structure, and have high directional anisotropy and hard deformation mode [8,9], resulting in limited ductility that hinders their applications. Although significant advances have been developed in fatigue mechanics, most of the previous studies on fatigue performance of Mg alloys rely on ex situ mechanical testing and microstructural characterizations [10–13]. These ex situ investigations cannot adequately resolve the relationship between the macroscopic mechanical behavior and microscopic mechanisms activated during cyclic loading. Recently, comprehensive studies have been performed to understand the low cycle fatigue (LCF) performance of wrought magnesium alloys using in situ neutron diffraction technique [14–16]. Most of these in situ works aim to identify the deformation mechanism sequence of the most widely used classes of Mg alloys, e.g., Mg–Al–Zn (AZ series)

---

* Corresponding author.
*E-mail address:* ygao7@utk.edu (Y. Gao).

https://doi.org/10.1016/j.msea.2021.140860
Received 13 October 2020; Received in revised form 19 December 2020; Accepted 25 January 2021

and Mg–Zn (Z series) [4–6]. The plastic deformation of wrought magnesium alloys at room temperature during cyclic loading is dominated by alternating twinning and detwinning mechanisms [4–6], which are strongly affected by the initial texture component as well as loading modes [5–7]. Despite these past studies, the selection of various deformation modes, together with their evolution, needs to be connected to a broader range of materials. Prior studies are limited mostly to solution strengthened Mg alloys with rolling texture. On the other hand, one subject with increasing interest is the effect of precipitation strengthening on the major slip systems, i.e., basal slip and prismatic slip, and extension twinning system in Mg alloys [17–21]. Different types of precipitates are proposed to have distinct effects on the anisotropy by affecting the critical resolved shear stress (CRSS) for different deformation modes in Mg alloys [18–20]. Robson et al. [19] proposed that the presence of c-axis rod-type precipitates in the Z5 (Mg-5 wt.% Zn) alloy increases asymmetry, while precipitation of the basal plates in AZ91 alloy reduces asymmetry. Whilst those understandings are based on the monotonic loading, to date, the influence of precipitates on the cyclic fatigue behavior and potential activated deformation modes are not well established. Similar to the above dependence of deformation behavior on precipitation, the resulting LCF performance should have a direct reliance on the chosen deformation mode transitions. A comparison to prior studies on purely solution strengthened Mg alloys along these lines will shed critical insights on the micromechanical understanding of LCF lifetime predictions.

The above issues must be understood on the microstructural length scales, leading to the ideal choice of in situ neutron diffraction measurements. The deep penetration capability of neutron beams enables the neutron diffraction technique to be an in situ, non-destructive probe method to determine the crystal structures, atomic spacing, and other structural information [22,23]. The shift of the diffraction peak position that yields the lattice strain is related to the inhomogeneous deformation on the grain scale (or called Type-II strain), while the peak broadening corresponds to the inhomogeneous deformation inside the grains (or called Type-III strain) [23]. In this study, the state-of-the-art in situ neutron diffraction measurement is employed to investigate the strain-controlled LCF behavior of the AZ80 alloy strengthened by the plate-type precipitates. The goal of this study is to investigate the effects of deformation history, initial texture, and, in particular, precipitates on plastic deformation during cyclic loading. Given the complicated deformation modes in Mg alloys, our attention will also be placed on the information regarding the relative significance of various twinning/detwinning/dislocation plasticity mechanisms during cyclic loading conditions.

## 2. Experimental details

### 2.1. Material

The AZ80 Mg alloy sample used in this study was cut from a commercially extruded flat bar with the T5 temper. The crystallographic texture of the as-extruded plate was determined using the synchrotron X-ray diffraction technique at the Advanced Photon Source (APS), beamline 11-ID-C, at Argonne National Laboratory. The sample for optical microscopy (OM) was mechanically polished and etched using a solution consisting of 10 ml $H_2O$, 100 ml ethanol, 5 ml acetic, and 1 g picric acid. Fig. 1 shows the OM image for the as-received AZ80 alloy on the longitudinal section. As seen, the measured average grain size of grains was about 15 ± 4 μm and β-$Mg_{17}Al_{12}$ precipitates are uniformed distributed on the Mg matrix after the aging treatment. These precipitates usually have a common Burgers orientation relationship (OR) $[1\bar{1}1]_\beta//[2\bar{1}01]_\alpha$, $(110)_\beta//(0001)_\alpha$ with the Mg matrix [24,25]. The content of the β-$Mg_{17}Al_{12}$ phase has been determined to be about 12.5% in this alloy by performing Rietveld refinement on the texture data obtained by the synchrotron X-ray diffraction. A dog-bone shaped sample with gauge dimensions of φ8mm × 16 mm was cut with the longitudinal axes parallel to the transverse direction (TD) of the flat bar.

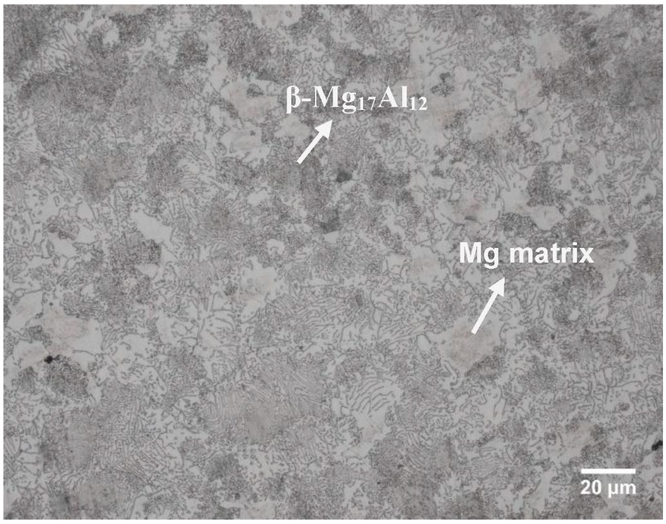

**Fig. 1.** Optical microscopy (OM) image for the initial microstructure of the AZ80 alloy with T5 temper.

### 2.2. In situ neutron diffraction measurements during LCF

In situ neutron diffraction measurement was performed at the VULCAN Engineering Materials Diffractometer [26,27], the Spallation Neutron Source (SNS), Oak Ridge National Laboratory (ORNL) under a continuous loading condition. In this study, the fully reversed strain-controlled LCF experiment was conducted at a total strain amplitude of ±1%, at room temperature with triangular loading waveforms. In situ neutron diffraction measurements were performed for the initial compression, 1st, 2nd, 5th, 10th, 20th, 50th, 70th, and 90th fatigue cycles. We adopted strain rates of $7.4 \times 10^{-6}$ $s^{-1}$ in the initial compression, 1st, and 2nd cycles and $1.11 \times 10^{-5}$ $s^{-1}$ in the remaining cycles where in situ neutron diffraction measurements were performed. The slow strain rate during these selected fatigue cycles did not affect the deformation behavior since creep was negligible at room temperature. In the other cycles, we used a fixed strain rate of $1 \times 10^{-2}$ $s^{-1}$.

The sample was mounted horizontally on an MTS load frame, with the loading direction (LD) along the transverse direction (TD) and the radial direction parallel to the ND of the sample, respectively. The angle between the incoming neutron beam and the specimen was 45°. The two stationary detector banks (axial detector bank and radial detector bank) are located at ± 90° to the incoming beam, simultaneously recording two complete diffraction patterns with diffraction vectors parallel ($Q\|$) and perpendicular ($Q\perp$) to LD. Therefore, the diffraction patterns along the axial and radial directions of the sample were recorded by axial detector bank and radial detector bank, respectively. The neutron beam slits were 7 mm (horizontal) × 7 mm (vertical), with a 5 mm receiving collimator, leading to a neutron gauge total volume of 245 $mm^3$. The neutron diffraction measurements were conducted under the high-intensity mode with a chopper frequency of 30 Hz with a center wavelength of 2.7 Å, which corresponds to a lattice d-spacing range of 0.9–3.2 Å. After the measurement, the data reduction was performed, using VULCAN Data Reduction and Interactive Visualization software (VDRIVE) [28]. The neutron diffraction data were chopped into time bins with a time interval of 3 min. The lattice (internal) strains of a given orientation (hk.l) plane to the detector banks can be calculated based on the peak shift between the loaded and load-free patterns, given by:

$$\varepsilon_{hk.l} = \frac{d_{hk.l} - d^0_{hk.l}}{d^0_{hk.l}} \tag{1}$$

where $d_{hk.l}$ and $d^0_{hk.l}$ are the plane d-spacings in the loaded and load-free conditions, respectively. The counting time for the undeformed sample was 10 min to reduce the propagated $d^0_{hk.l}$ statistic error.

## 3. Results

### *3.1. Material texture*

The crystallographic texture of the extruded plate by synchrotron X-ray diffraction is displayed in Fig. 2(a). Different from traditional rolling and extruded Mg alloys, the initial texture of the current AZ80 alloy exhibits a combined feature of typical rolling and extrusion textures, with two major texture components, one with the basal plane of the HCP structure parallel to the normal direction (ND) and the other with the basal plane parallel to the TD of the extruded flat bar. The former texture component is much stronger than the latter. The neutron diffraction patterns for the initial state and completely tensile unloading state in the 70th cycle are exhibited by Fig. 2(b) and (c), respectively, from which two sets of diffraction peaks are shown: the peaks marked with the red cycle belong to the $\beta$-$Mg_{17}Al_{12}$ phase, and the others pertain to the Mg matrix. By comparing these two diffraction patterns, no obvious difference in the relative diffraction intensity, especially for {00.2} and {10.0} peaks, are observed. This fact indicates that the texture under the tensile unloading state will recover to the initial state during cyclic straining. According to the polar nature of the twinning, the {00.2} and {10.0} grains in the axial detector bank are favorably oriented for the {10.2} extension twinning in tension and compression, respectively, under current loading condition that LD along with the TD. It is reasonable to anticipate that the initial texture in this alloy can give rise to a more complicated deformation mode sequence during cyclic loading than that in previous studies [4–7,29].

### *3.2. Macroscopic mechanical behavior*

The hysteresis loops of the selected fatigue cycles for the in situ neutron diffraction measurement are plotted in different colors, as shown in Fig. 3(a). The asymmetric hysteresis loops are primarily ascribed to the formation of the {10.2} extension twins during the compressive loading and detwinning during the subsequently reversed loading [4,6]. Fig. 3(b) exhibits the peak stress and 0.2% proof stress in each fatigue cycle. Slight strain hardening is observed on the tensile peak stress evolution, and the compressive peak stress is almost saturated. Note that the 0.2% proof stress in the reverse tension side exhibits a much smaller value than that in the compression side in each fatigue cycle, which can be explained by the early onset of detwinning [4]. The mechanical stress-strain responses in the 1st cycle and 70th cycle are displayed in Fig. 3(c) and (d), respectively. Small pseudo-elastic strains are observed upon tensile and compressive unloading, which are reported to be related to the reactivation of basal slip [16,30]. In particular, upon tensile reloading in the first cycle, right after 0% strain, an inflection with an increased slope (hardening rate) is observed. The different shapes of the hysteresis loop for the 1st and 70th cycles in the tensile side are quite, as shown in Fig. 3(c) and (d), which indicates different deformation mode sequences in these two fatigue cycles.

### *3.3. Microscopic response by neutron diffraction*

#### *3.3.1. Diffraction intensity evolution*

The diffraction intensity evolutions of certain hk. ls in both the axial and radial directions in the selected fatigue cycles are presented in Fig. 4 (a) and (b), respectively. The occurrence of {10.2} extension twinning leads to a sudden re-orientation of grains at about 86.3°, which converts the {00.2} grains into {10.0} grains during loading in tension, and vice versa in compression [4,6]. Consequently, the diffraction intensity variations in twin-related grains can be used to identify the {10.2} extension twinning process [4,6,29]. It should be pointed out that the {11.0} and {10.3} grains are also in {10.2} extension twin-related orientations [31]. Upon initial compression, {10.2} extension twinning initiates at a strain of $\sim -0.5\%$, where the diffraction intensity of the {00.2} grains starts to increase in the axial detector bank and decrease in the radial detector bank. While during reverse tension, the diffraction intensity of {00.2} gradually decreases, accompanying with the increase of diffraction intensity of the {10.0} grains in the axial detector bank, which indicate the detwinning behavior [4]. The cyclic increase-decrease (or decrease-increase) sequence in the diffraction intensity of {00.2} (or {10.0}) grains manifests that the alternative twinning and detwinning deformation occur during the compression-tension sequence in each fatigue cycle. It can be seen that

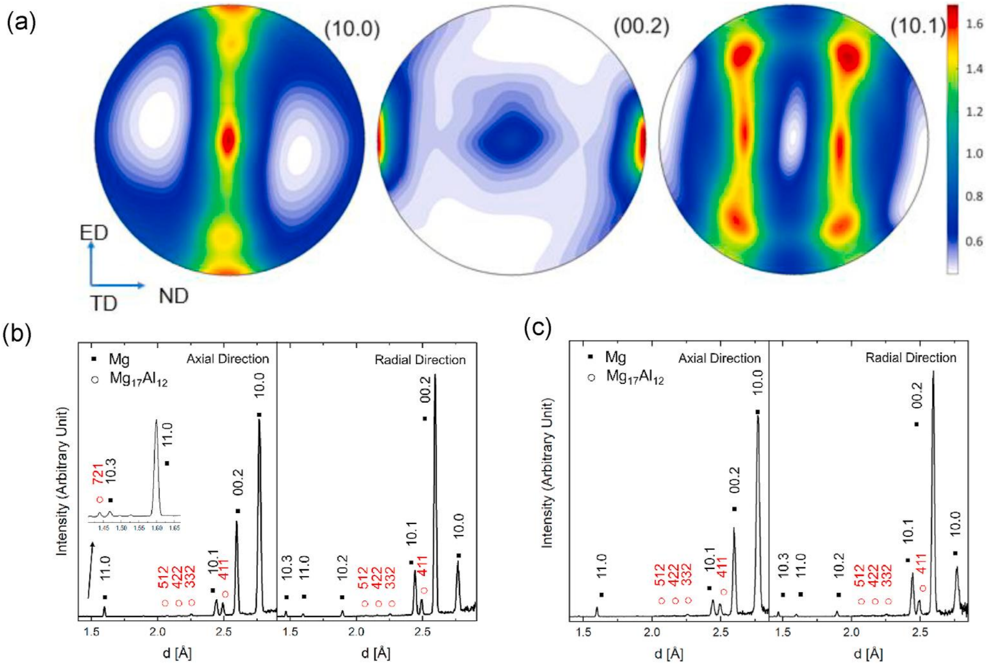

**Fig. 2.** (a) The initial texture of the AZ80 alloy measured by ex situ synchrotron X-ray diffraction, which exhibits a combined feature of typical rolling and extrusion textures, with two major texture components, one with the basal plane of the HCP structure parallel to the normal direction (ND) and the other with the basal plane parallel to the transverse direction (TD) of the extruded flat bar, (b) and (c) the neutron diffraction pattern under as-received and complete tensile unloading state in the 70th cycle of the AZ80 alloy, respectively.

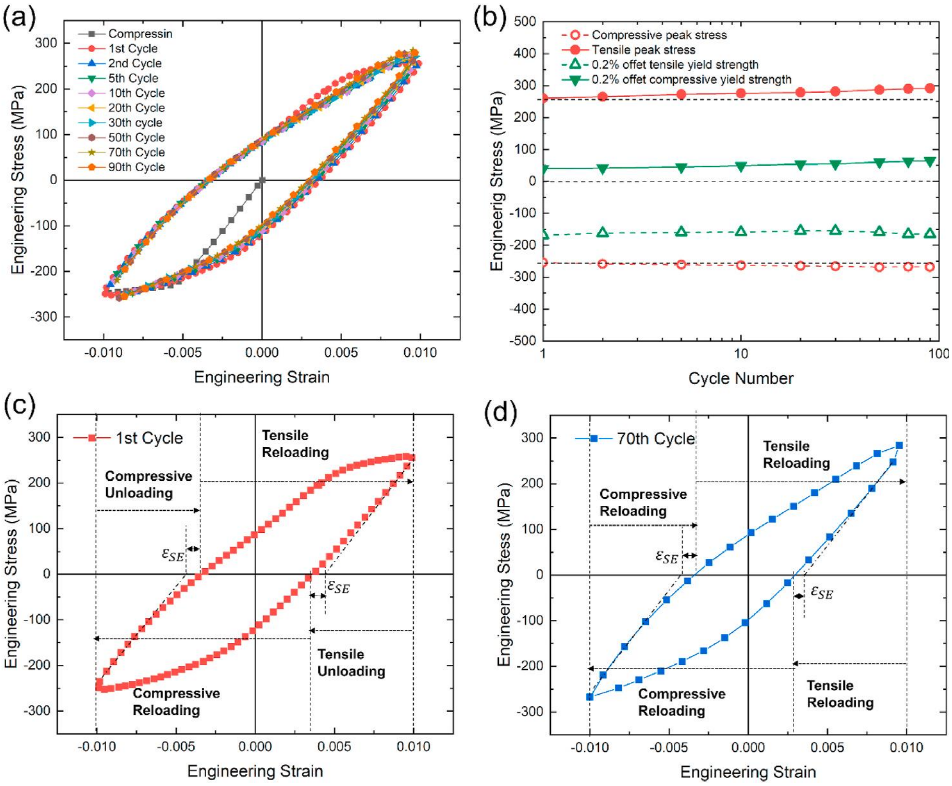

**Fig. 3.** (a) Asymmetric hysteresis loops loaded along the prior transverse direction for selected cycles, (b) the peak and 0.2% offset yield stress as a function of fatigue cycles, (c) and (d) the hysteresis loops of the 1st and 70th cycle, respectively, which are divided into four loading stages: compressive loading, compressive unloading, tensile reloading, and tensile unloading.

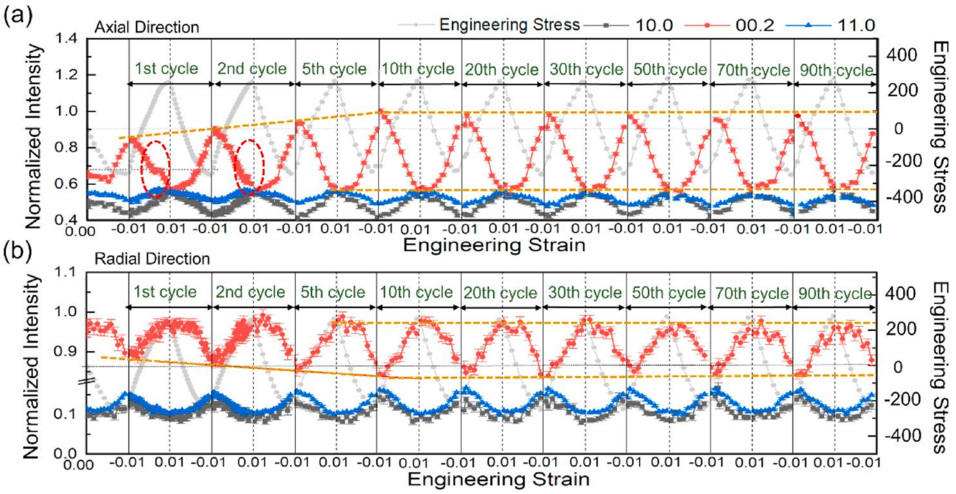

**Fig. 4.** The diffraction intensity evolution of certain hk. ls in selected fatigue cycles for (a) the axial detector bank, and (b) the radial detector bank.

the diffraction intensity of the {00.2} grains in LD at the minimum strain, −1%, increases progressively in the first 5 cycles before saturating. This suggests that a progressively increasing number of {10.0} grains are involved in the {10.2} extension twinning during the first 5 cycles, and then cease changing in the following fatigue cycles [7]. It is worth noting that the significantly increased diffraction intensity in the {00.2} grains at a strain of −1% in the 1st cycle is partly due to the different compressive strain levels [6], i.e., −1% for the initial compression, and ~1.3% for the first cycle. Nevertheless, different from previous reports [4,29], two plateau values appear on the diffraction intensity evolution curve in the first two cycles under reverse tension, noted with a red dash cycle in Fig. 4(a), which will be illustrated in the following.

Fig. 5 shows the diffraction intensity evolution of {00.2} grains in LD as a function of engineering stress during cyclic loading. “T”, “D”, “DT”, and “TDD” refer to twinning, dislocation, detwinning, and transition from detwinning to dislocation, respectively. In this paper, “T1” and “T2” refer to the {10.2} extension twinning in the parent grains whose original c-axis is perpendicular and parallel to LD, respectively. “DT1” and “DT2” refer to the detwinning process from “T1” and “T2” twinned grains, respectively. The slopes of the diffraction intensity with applied stress curves can provide the information regarding the deformation modes in wrought Mg alloys [6,7]: in LD, the increase of {00.2} diffraction intensity under compression is related to the

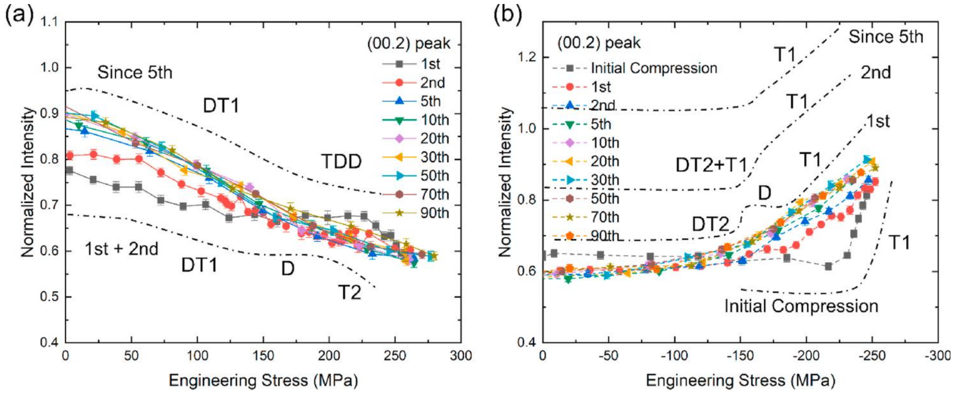

**Fig. 5.** The diffraction intensity variation of {00.2} grains as a function of engineering stress in selected fatigue cycles (a) during tension, and (b) during compression in the axial detector bank.

twinning/detwinning process, the decrease of {00.2} diffraction intensity upon tension corresponds to the detwinning/twinning process, and the plateau regime of {00.2} diffraction intensity with stress associates with the dislocation-controlled mode. The general trends of these curves are represented by the dashed lines in Fig. 5.

As shown in Fig. 5(a), the {00.2} diffraction intensity under tension in the first two cycles decreases initially, but gradually reaches a constant value, and subsequently decreases sharply again. According to the initial texture, the decrease in {00.2} diffraction intensity can be related to the detwinning in the twinned {00.2} grains or the twinning in the "parent" {00.2} grains. The constant regime is related to the dislocation-controlled mode. The detwinning process is reported to initiate more easily than the twinning process [4], presumably because detwinning is a mechanism of shrinking existing twins, which does not require twin nucleation [9]. Therefore, the first decrease region is related to the detwinning (DT1) mode, and the second one corresponds to the twinning (T2) mode. Consequently, the plastic deformation during tension in the first 2 cycles is thus controlled by the detwinning (DT1) mode, dislocation (D) mode, and twinning (T2) mode. The same diffraction intensity level in the constant region upon tension in the 1st cycle with that in the undeformed state further, seen in Fig. 5(a), illustrates that the detwinning (DT1) is fully exhausted. Since the 5th cycle, the {00.2} diffraction intensity initially undergoes a rapidly decreased region and then a slowly decreased region by the end of tension that corresponds to the transition for detwinning to dislocation (TDD) mode where the detwinning is almost exhausted and dislocation rule over instead of the activation of twinning (T2). Therefore, the plastic deformation since the 5th cycle is dominated by the detwinning (DT1) mode and then transition from detwinning to dislocation (TDD) mode. The prolonged detwinning process in the following cycles suggests that the range of detwinning-controlled (DT1) region strongly depends on how many grains are involved in the prior twinning process in each fatigue cycle.

Fig. 5(b) shows the diffraction intensity evolution of {00.2} grains upon compression. During the initial compression, the plastic deformation is dominated by the extension twinning (T1) process [6]. The twinned {00.2} grains formed in the initial compression process, however, are not enough for the consumption of the subsequent detwinning process, leading to the premature end of the detwinning mechanism and the beginning of the dislocation-controlled mode, as displayed in Fig. 5 (a). The {00.2} diffraction intensity shows a trend of initial increase, then becomes stable, and followed by another increase during compression in the 1st cycle, similar to the analysis of the deformation mechanism during tension in the first two cycles, which correspond to the detwinning (DT2) mode, dislocation (D) mode after fully detwinning (DT2), and twinning (T1) mode, respectively. The {00.2} diffraction intensity undergoes a rapid increase to a slow increase during compression in the 2nd cycle. The initial rapidly increased region is proposed to be related to the combination of detwinning mode (DT2) and extension twinning (T1) mode, and the slowly increased region corresponds to the sole extension twinning (T2) mode due to the exhaustion of detwinning (DT2). From the 5th cycle, the plastic deformation is quite identical to the initial compression, solely controlled by twinning (T1) mode, as displayed in Fig. 5(b). Obviously, the twinning (T1) process is the dominant deformation mechanism upon compression.

### 3.3.2. *Lattice strain evolutions*

The lattice strain evolutions of {10.0}, {10.3}, {00.2} and {11.0} grains of the Mg matrix, and {411} grains of the β-$Mg_{17}Al_{12}$ phase in the initial compression, 1st cycle, and 70th cycle are shown in Fig. 6. The inflection points in the lattice strain with applied stress curves can be attributed to the activation of specific deformation mechanisms. In general, the lattice strain of given grains groups diverging vertically suggests that these "soft" grain families begin to accommodate plastically, and simultaneously the "hard" grain families start to share the more elastic load, causing a divergence with a small slope. The lattice strain variations can be understood by considering the Schmid factors for the basal slip and {10.2} extension twinning for the given set of grain orientations [31]. The different deformation-controlled regions are separated by the square-dashed lines and the elastic line for Mg alloy and the {411} grains corresponds to the dash-dotted lines in Fig. 6.

During initial compression, it is clear from Fig. 6(a) that all the grain orientations have a similar slope in the initial elastic deformation owing to the near-elastic isotropy of Mg and its alloys [4]. The {10.1} and {10.3} grains yield first with the corresponding curve diverging from the linear response due to the activation of basal <a> slip at relatively low stress [32]. Correspondingly, other hard grains begin to accommodate more load with a smaller slope. All the lattice elastic strain curves show a strong inflection at the macroscopic yield stress of ~228 MPa, where the {10.2} extension twinning is activated. Once the twinning is activated, the {00.2} and {10.3} grains in the LD begin to accommodate more loads with a decreased slope, while the {10.0} and {11.0} grains are relaxed which depart from the linear response. Kada et al. [33] suggested that the β-$Mg_{17}Al_{12}$ phase has a higher directional modulus of 69 GPa along (100) direction and a lower directional modulus of 52 GPa along (111) direction, whilst Gharghouri et al. [8] reported a high diffraction elastic constant of 87 GPa along (111) direction. In this study, the diffraction elastic constant for the {411} grains is determined to be ~57 GPa, which is among the range of the elastic moduli of the β-$Mg_{17}Al_{12}$ phase suggested by Kada et al. [33]. The departure from the elastic response is noticed at ~118 MPa in the {411} grains, where the basal slip activates. With further increase in the applied stress, the lattice strain of {411} grains varies almost linearly with stress until an increased rate of the lattice strain accumulation is observed after yielding.

As for the 1st cycle, upon reverse tensile loading [Fig. 6(b)], the

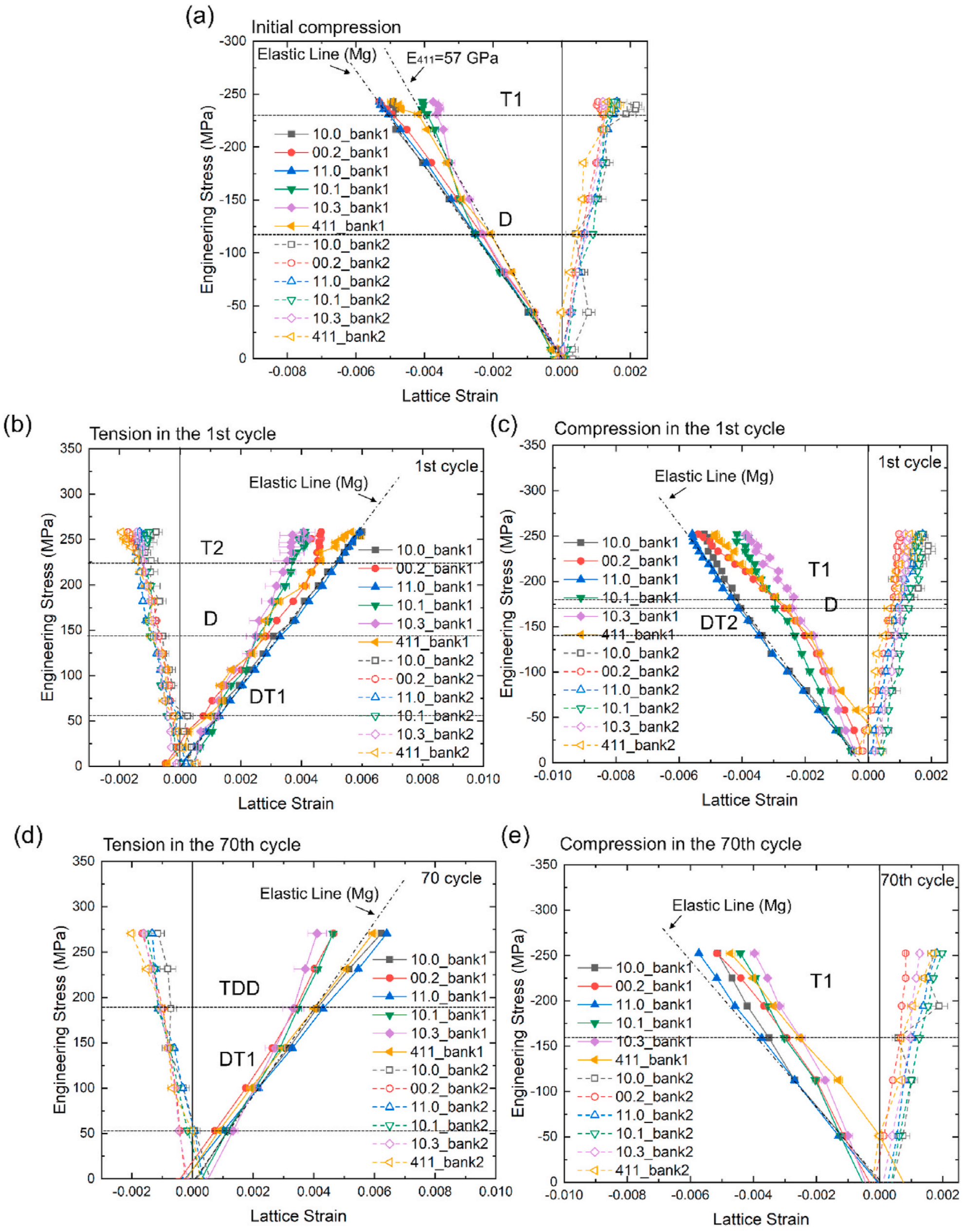

**Fig. 6.** Lattice strain evolution of certain interested hk. ls during (a) the initial compression, (b) tension and (c) compression in the 1st cycle, and (d) tension and (e) the compression in the 70th cycle.

lattice strain responses of certain grain groups in LD during different deformation mode regions are distinct. During the detwinning-controlled (DT1) region where the {10.0} and {10.1} diffraction intensity increase, and {00.2} diffraction intensity decreases, the {10.0} and {10.1} grains share more loads, and the {00.2} grains yield. During the dislocation-controlled (D) region where the {00.2} diffraction intensity keeps constant in Fig. 5(a), the {10.1} and {10.3} grains yield immediately. With the increase of stress, the sample then suddenly undergoes a twinning-dominated (T2) region where the {00.2} diffraction intensity decreases dramatically and the lattice strains of the {00.2} and {10.3} grains diverges vertically because these grains are relaxed relative to the stress field in the surrounding grains. During compression in the 1st cycle in Fig. 6(c), the general trend of lattice strain evolution is identical to that in the initial compression except for the occurrence of detwinning-controlled (DT2) mode. Once detwinning (DT2) is active, the {00.2} and {10.3} grains begin to accommodate more loads with lower slopes, coupled with the {00.2} diffraction intensity decreasing [Fig. 5(b)]. It is noted that the {411} grains share a larger portion of loads since the activation of detwinning (DT2).

The lattice strain evolutions of certain grain orientations in the 70th cycle are shown in Fig. 6 (d) and 6(e). During tension, the plastic deformation is controlled by detwinning-controlled (DT1) mode and transition from detwinning to dislocation-controlled (TDD) mode, sequentially. The {10.1} and {10.3} grains that favor basal slip begin to yield at ~190 MPa due to the activation of TDD mode, where a large portion of twinned grains is consumed by the detwinning process and dislocation motion become more active. During compression, the general trend of lattice strain evolution is identical to that in the initial compression in Fig. 6(a).

## 4. Discussion

### 4.1. Deformation mechanisms

The deformation modes during plastic deformation have been divided by the peak stress, 0.2% proof stress, and transition stress in Fig. 7, in which the T1, T2, DT1, DT2, D, and TDD-controlled regions are distinguished by different patterns. Apparently, the complicated deformation mode sequence can be seen in the first two cycles, which are closely related to the initial texture with two major texture components in this AZ80 alloy. However, the deformation mode sequence in the following cycles becomes similar to that of Mg alloys with simple rolling or extruded texture [4,6].

The tension following compressive deformation occurs predominantly by detwinning initially. This is consistent with previous reports in the literature [9,34,35]. The detwinning process is significantly influenced by the twinning processes that take place during prior compression. The occurrence of dislocation-dominated (D) deformation region in the first two fatigue cycles can be explained by the relatively early exhaustion of the detwinning process, as the inadequate twinned grains formed in the previous compression have been completely consumed by the detwinning before the strain reaches +1% in the first two cycles. Nevertheless, the sufficient twinned grains for consumption by detwinning lead to the disappearance of dislocation-controlled (D) mode in the following cycles. The dislocation (D) mode, activated after detwinning, may correspond to the activation of basal <a>-type slips, non-basal <a>-type slips (i.e., prismatic), or <c + a>-type slips. As the CRSS for extension twinning is reported between the non-basal slip and basal <a> slip [32,36], the dislocation (D) mode here therefore is ascribed to the basal <a> slip in the soft grains (i.e., {10.2, {11.2}, and {10.1} grains). In this region, the rapid strain-hardening behavior exhibiting in the macroscopic response in this region [Fig. 3(c)] can be explained by the composite effect in the sense that only a small number of grains undergo plastic deformation and the rest remain elastic [16, 37]. The onset of detwinning (DT1) at a relatively low-stress level and dislocation-controlled (D) deformation at a relatively high-stress level produces an S-shaped hardening curve [Fig. 3(c)].

The compressive deformation is predominantly controlled by twinning (T1) in the whole fatigue cycles. The detwinning mode (DT2) in the first two cycles arises from the detwinning process in the {10.0} twinned grains that are obtained in the prior tension. Similarly, the basal <a> slip is proposed to be the dominant deformation mechanism in the dislocation-controlled (D) region.

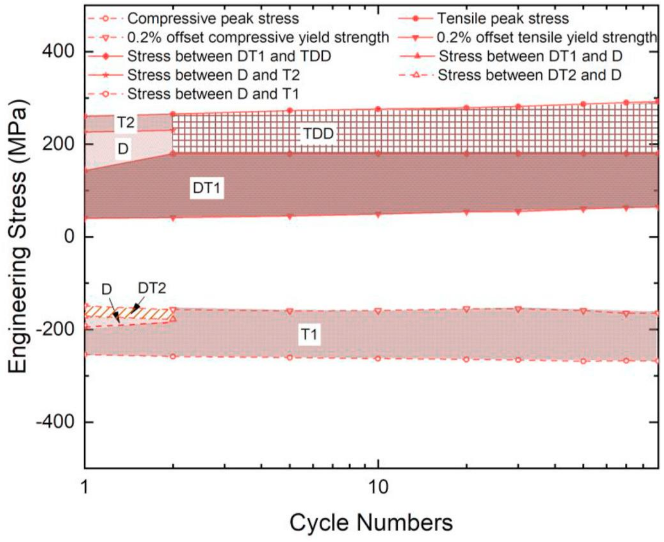

**Fig. 7.** The peak stresses, 0.2% proof stresses, stresses at the dividing points between twinning/dislocation, detwinning/dislocation, and detwinning/transition region, and deformation modes as a function of the number of cycles.

It is interesting to note that, although the texture after total tensile unloading is identical to that in the initial state [Fig. 2], the extension twinning-controlled (T2) mode only occurs in the first 2 cycles. This fact can be explained by that the CRSS for twinning is not reached during tension in the following cycles, if assuming that twinning is activated by a CRSS. In fact, by comparing Fig. 6(b) and (d), it can be seen that the accumulated lattice strain in {00.2} grains at the end of the tension in the 70th cycle is still less than that for the twinning onset, ~0.046, in the 1st cycle. This trend makes sense since when detwinning (DT1) is the deformation mechanism, the lattice strain of the "soft" {00.2} grains diverges vertically, leading to the slower lattice strain building up. As more and more grains are involved in the twinning (T1) and sequent detwinning (DT1) process in the first 5 cycles, a large portion of shear stress fields in the {00.2} grains are relieved by the enlarged detwinning process (DT1) during tension, resulting in the insufficient accumulated shear stress for the onset of extension twinning (T2). Therefore, the disappearance of the twinning (T2) mode in the following cycles can be explained by the fact that the CRSS for twinning is not reached due to the prolonged detwinning (DT1) process. Consequently, it can be concluded that the deformation mode sequence strongly depends upon deformation history and texture during cyclic loading for Mg alloys. These observations are further validated by comparing to literature studies on pre-deformed Mg alloys by Cáceres et al. [38] and Drozdenko et al. [39].

In previous studies [4–7], solution-strengthened Mg alloys with different texture display quite different deformation mode sequence as opposed to our Fig. 5. The material in this work has a combined rolling/extrusion texture and precipitation strengthening for basal slip systems, which are responsible for the observed elevated dislocation activities. One question that naturally arises is on the connection between results such as in Fig. 5 and LCF lifetime. Despite a lack of predictive models, our previous study on pre-twinned AZ31B Mg alloy [7] may offer some valuable insights. The pre-twinned sample will experience almost no dislocation activities on a similar plot like Fig. 5, and it has a much superior LCF lifetime than the sample without pre-twinning. On the other hand, Fig. 5 here displays more pronounced dislocation activities than either pre-twinned or no pre-twinned AZ31B (that has no precipitates). Dislocation activities during cyclic loading tend to form persistent slip bands that serve as damage sites for fatigue crack initiation. Consequently, these comparisons between this work and prior ones [4–7] provide a micromechanical basis for model development of LCF lifetime.

### 4.2. Precipitation hardening effect on twinning

In the polycrystalline case, a number of attempts have been made to increase the CRSS for twinning. It is well accepted that the activation of twinning is controlled by a CRSS, which can be estimated by the Schmid law under a uniaxial loading condition, described by Ref. [4]:

$$\tau_{CRSS} = \sigma_c cos\lambda cos\phi \tag{2}$$

where λ and φ are the angles between the loading axis and the twin plane normal and twin direction, $\tau_{CRSS}$ is the CRSS, and $\sigma_c$ is the critical applied stress. Using Eq. (2), a CRSS of ~91 ± 5 MPa is yielded for {10.2} extension twinning in this AZ80 alloy with a Schmid factor of ~0.40. The CRSS obtained here is quite close to that in the Mg-7.7 at.% Al alloy (65–75 MPa) [40]. Wu et al. [4] reported a CRSS value of 15 MPa in the AZ31 alloy. This fact suggests that the value of CRSS is related to the precipitates, due to the strengthening effect of precipitates on the activation of twinning. The twinning-controlled compressive yield stress of a solution-treated AZ80 alloy with similar grain size is reported to be ~145 MPa [41]. According to Eq. (2), an estimated CRSS increment of ~33 MPa can be calculated attributed to the precipitation strengthening effect, which is comparable with that in the AZ91 alloy after and before aging treatment [33,42]. However, the correction should be made by considering the loss of solute strengthening despite the negligible change in the grain structure and texture caused by aging can be ignored. For the AZ series Mg alloys, a reduction of ~10 MPa in the CRSS increment is reported [19]. The β-$Mg_{17}Al_{12}$ phase deforms elastically under cyclic loading, which cannot be cut through by twins or dislocations [19]. Robson et al. [20] proposed that twins will engulf some of the precipitates during propagation when the precipitates are small with a fraction volume between $2-10\%$ (~12.5% in the current case). This will introduce a strain incompatibility at the particle-matrix interface with a maximum value of ~6.5% [43]. The back stress arising from the strain incompatibility can result in the strengthening effect in twinning [19], although it can be reduced by the local plastic deformation [43].

### 4.3. Evolution of load sharing

During the twinning/detwinning dominated deformation under compression, the {00.2} twinned grains in the axial direction tends to yield a smaller slope of the lattice stress/strain curve than the calculated linear elastic response, 48 GPa [35]. This can be explained by the fact that although the newly formed {00.2} twinned grains are relaxed relative to the matrix due to the small c/a ($<\sqrt{3}$) ratio of magnesium, the existing {00.2} grains have to accumulate strain more rapidly than the aggregate as a whole because they are in a “hard” orientation for both the twinning and basal slip [35]. Therefore, the lattice strain builds up faster than linear elasticity due to load sharing with the existing {00.2} grains and surrounding grains. During the twinning/detwinning-dominated deformation region upon tension, loads transfer from the “soft” {00.2} grains for twinning and detwinning to surrounding grains. The work hardening effect in the twinning and detwinning-dominated regions is limited, and the transition from detwinning to the dislocation-dominated (TDD) deformation and dislocation-dominated (D) regions exhibit a relatively large hardening response [7].

As the low volume fraction of precipitates in heat-treatable Mg alloys, reports on the load sharing effect of precipitates during cyclic loading are limited [33]. In the present case, however, a load sharing effect of the precipitates is suggested. Once the activation of plastic deformation, the β-$Mg_{17}Al_{12}$ phase begins to accommodate a larger portion of the loads. However, Bhattacharyya et al. [44] suggested that the load sharing provided a limited strengthening effect due to the modest phase fractions and stiffness difference between the matrix and precipitates. The fractured surface after LCF obtained by scanning electron microscopy (SEM) is shown in Fig. 8, which consists primarily of ductile dimples within the grains formed as a consequence of microvoid coalescence [45]. The fatigue striations can be observed in Fig. 8 (b), which are a typical characteristic of fatigue crack propagation in ductile materials. To moderate the strain discontinuity between the elastically deformed unsheared precipitates and the Mg matrix, plastic relaxation effects, i.e., dislocation pileup, develop around these precipitates [43]. The local stress concentration near the weakly bonded particle-matrix interface facilitates the microvoid creation and their coalescence forming dimples, which offers a great opportunity for the formation and propagation of cracks and degrades fatigue life [45].

### 4.4. Iso-strain model

To explain the evolution of the orientation-dependent lattice strains through the elastic-plastic transition regime and the macroscopic stress level at which yielding begins on average, the iso-strain model was applied [46]. The deformation systems of materials are specified by the crystal structures. For the Mg alloys with an HCP crystal structure, the plastic deformation is usually controlled by the basal slip, prismatic slip, pyramidal slip, and twinning [16]. In our case, according to the above analysis, only basal slip and extension twinning are considered. As the elastic deformation in Mg alloys is quite isotropic [4], the Hooke’s law for an isotropic material (or an elastically isotropic aggregate) can be used directly by $E=\frac{\sigma}{\varepsilon}$, where the $\sigma$ is true stress, $\varepsilon$ is the true strain, and E is Young’s modulus. Consider a number of {10.0}, {00.2}, {10.1}, {11.0}, and {10.3} grains all of which under the same strain, as schematically displayed in Fig. 9(a) and distinguished by different colors.

The Schmid factors, $m^{hk.l}$, of basal slip and extension twinning for certain grain orientations under a uniaxial loading condition are listed in Table 1. The calculation process of the Schmid factor is in detail in the Appendix. The directional strength measure, $S^{hk.l}$, for a certain grain orientation, hk.l, under a uniaxial loading is therefore defined as [46–48]:

$$S^{hk.l}=\frac{1}{m^{hk.l}}\times\frac{E^{00.1}}{E^{hk.l}}\approx\frac{1}{m^{hk.l}} \tag{3}$$

The last approximation arises because the degree of elastic anisotropy is very weak for Mg alloys. For each deformation mode, the values of $S^{hk.l}$ for different grain orientations calculated based on the maximum value of the Schmid factor are listed in Table 2. Generally, for a specific deformation mode, the high values of $S^{hk.l}$ suggest the “hard” grain orientations that are not favorably oriented for slip or twinning and are associated with high strength; the low values of $S^{hk.l}$, conversely, correspond to the “soft” grain orientations associated with low strength and earlier yield. It is worth mentioning that the grain orientations with the negative $S^{hk.l}$ values for twinning are unable to respond to the corresponding twinning modes under current load conditions, which belong to “hard” orientations for twinning, while the absolute value of $S^{hk.l}$ for dislocation slip modes. Consequently, under iso-strain condition, the soft grains with small $S^{hk.l}$ values of a certain deformation mode yield first, as shown in Fig. 9(b).

From Table 2, it is clear to see that the {10.1} and {10.3} grains have much smaller $S^{hk.l}$ values compared with other orientations under both compression and tension for basal slip, suggesting that these grains are in “soft” orientations for basal dislocations. The deformation mode with relatively smaller CRSS will initiate earlier and the CRSS for basal slip is

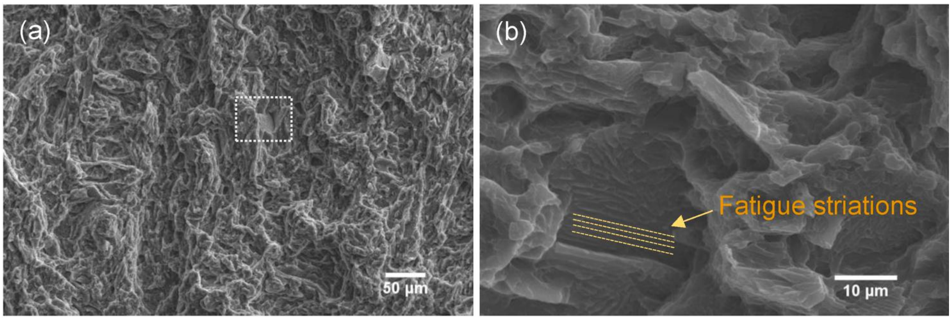

**Fig. 8.** (a) Scanning electron microscopy (SEM) micrographs showing the fracture surfaces after low-cycle fatigue (LCF) (1% strain amplitude), and (b) is the magnified images taken from the regions surrounded by white dashed line in Fig. 8 (a).

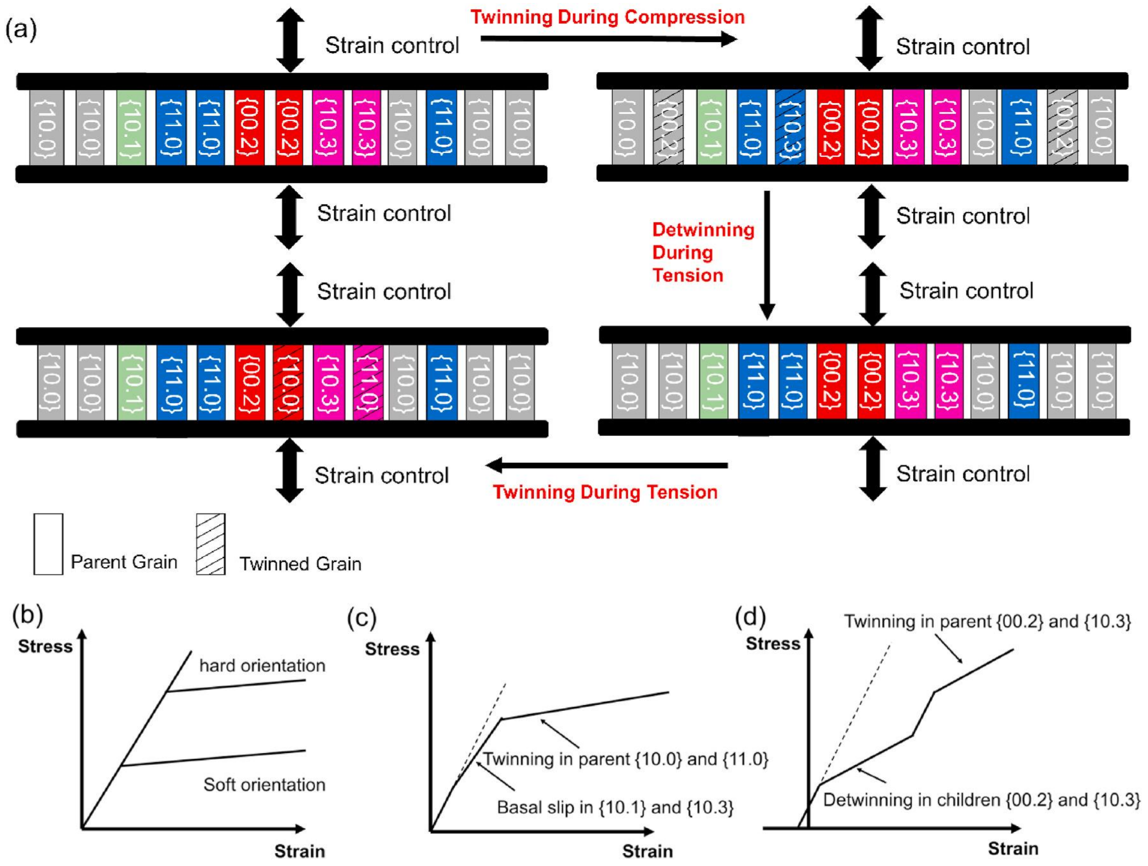

**Fig. 9.** (a) A schematic pattern for the evolution of grain orientations during a compression-tension loading sequence, distinguished by different colors, loaded in the uniaxial condition between rigid plates, which results in an iso-strain condition for these grains, (b) individual stress-strain response of "soft" and "hard" grains for a certain deformation mode, (c) combined stress-strain response of during initial compression, and (d) combined stress-strain response during reverse tension in the first cycle. (For interpretation of the references to color in this figure legend, the reader is referred to the Web version of this article.)

**Table 1**
The Schmid factors, $m^{hk.l}$, of basal slip and extension twinning in Mg alloys for certain grain families under uniaxial loading condition.

| Deformation mode | Reflection | Compression | | | | | Tension | | | | |
|---|---|---|---|---|---|---|---|---|---|---|---|
| | | $10\bar{1}0$ | $10\bar{1}1$ | $11\bar{2}0$ | 0002 | $10\bar{1}3$ | $10\bar{1}0$ | $10\bar{1}1$ | $11\bar{2}0$ | 0002 | $10\bar{1}3$ |
| Extension Twinning/ Detwinning | $(10\bar{1}2)[\bar{1}011]$ | 0.499 | 0.305 | 0.374 | -0.499 | -0.190 | -0.499 | -0.305 | -0.374 | 0.499 | 0.190 |
| | $(01\bar{1}2)[0\bar{1}11]$ | 0.125 | 0 | 0.374 | -0.499 | -0.309 | -0.125 | 0 | -0.374 | 0.499 | 0.309 |
| | $(\bar{1}102)[1\bar{1}01]$ | 0.125 | -0.027 | 0 | -0.499 | -0.338 | -0.125 | 0.027 | 0 | 0.499 | 0.338 |
| | $(\bar{1}012)[10\bar{1}1]$ | 0.499 | 0.251 | 0.374 | -0.499 | -0.248 | -0.499 | -0.251 | -0.374 | 0.499 | 0.248 |
| | $(0\bar{1}12)[01\bar{1}1]$ | 0.125 | -0.027 | 0.374 | -0.499 | -0.338 | -0.125 | 0.027 | -0.374 | 0.499 | 0.338 |
| | $(1\bar{1}02)[\bar{1}101]$ | 0.125 | 0 | 0 | -0.499 | -0.309 | -0.125 | 0 | 0 | 0.499 | 0.309 |
| | **MAX** | 0.499 | 0.305 | 0.374 | -0.499 | -0.190 | -0.125 | 0.027 | 0 | 0.499 | 0.338 |
| Basal <a> Slip | $(0001)[2\bar{1}\bar{1}0]$ | 0 | -0.360 | 0 | 0 | -0.389 | 0 | 0.360 | 0 | 0 | 0.389 |
| | $(0001)[\bar{1}2\bar{1}0]$ | 0 | 0 | 0 | 0 | 0 | 0 | 0 | 0 | 0 | 0 |
| | $(0001)[\bar{1}\bar{1}20]$ | 0 | 0.360 | 0 | 0 | 0.389 | 0 | -0.360 | 0 | 0 | -0.389 |
| | **MAX** | 0 | 0.360 | 0 | 0 | 0.389 | 0 | 0.360 | 0 | 0 | 0.389 |

the lowest in Mg alloys [16,32]. This explains the initial inflection in the {10.1} and {10.3} lattice strain in Fig. 6(a). For the extension twinning mode under compression, the ranking from soft to hard orientations is {10.0}, {11.0}, {10.1}, {00.2} and {10.3}, sequentially. Therefore, the divergences in the lattice strains of the {10.0} and {11.0} grains are observed in the extension twinning controlled region in Fig. 6(a). The formation of the twinned grains with {00.2} and {10.3} orientations related to the twinning process is schematically shown in Fig. 9(a). The combined stress-strain response under initial compression is presented in Fig. 9(c). Once the basal slips are active in the {10.1} and {10.3} grains, the slope of the stress-strain curve tends to decrease slightly due to the small amount of {10.1} and {10.3} grains. After the activation of extension twinning in the {10.0} and {11.0} grains, the slope of the stress-strain curve decreases dramatically.

During the reverse tension in the first cycle, the {00.2} and {10.3} grains are in "soft" orientations for both the detwinning and twinning. The detwinning process with relatively low CRSS causes the initial inflection in the lattice strain of the twinned {00.2} and {10.3} grains [4, 9], and the lattice strain divergence in these grains at relatively high stress is due to the onset of twinning, as displayed in Fig. 6(b). The

**Table 2**
Directional strength measures, $S^{hk.l}$, of for major slips and extension twinning in Mg alloys for certain grain families under uniaxial loading condition.

| Deformation mode | Reflection | Compression | | | | | Tension | | | | |
|---|---|---|---|---|---|---|---|---|---|---|---|
| | | $10\bar{1}0$ | $10\bar{1}1$ | $11\bar{2}0$ | 0002 | $10\bar{1}3$ | $10\bar{1}0$ | $10\bar{1}1$ | $11\bar{2}0$ | 0002 | $10\bar{1}3$ |
| Extension Twinning/ Detwinning | $\{10\bar{1}2\}$<br>$< 10\bar{1}1 >$ | 2 | 3.27 | 2.67 | -2 | -5.26 | -8 | 37.04 | ∞ | 2 | 2.96 |
| Basal <a> Slip | $\{0001\}$<br>$< \bar{1}2\bar{1}0 >$ | ∞ | 2.78 | ∞ | ∞ | 2.57 | ∞ | 2.78 | ∞ | ∞ | 2.57 |

change in the grain orientations for detwinning and twinning during tension is also schematically shown in Fig. 9(a). It should be pointed out that the basal slips in the {10.1} and {10.3} grains can even initiate during the previous compressive unloading process [16,30] and remain active in the whole reverse tension. The combined stress-strain response during reverse tension in the first cycle is exhibited in Fig. 9(d). The slope of the stress-strain curve dramatically decreases corresponding to the activation of the detwinning and twinning process, respectively, and recovers in the basal slip-dominated region. There is no essential difference between Fig. 6(b) and (d), and between 6(c) and 6(f), which suggests that the local environment of twinning, detwinning, and retwinning is essentially the same.

## 5. Conclusions

In situ neutron diffraction was employed in the current study to investigate the deformation mechanisms of an extruded AZ80 Mg alloy at the grain level during the fully reversed strain-controlled LCF. Major conclusions can be drawn based on the present research, as described below:

(1) The initial texture and deformation history played an important role in the mechanical behavior of Mg alloys under a uniaxial loading condition. The occurrence of extension twinning during both compression and reverse tension in the first two cycles was ascribed to the initial texture with two major texture components in this alloy.

(2) Upon compression, plastic deformation was mainly dominantly by twinning with a limited basal slip for compatibility. More and more grains were involved in the twinning and the following detwinning process in the first 5 cycles. The CRSS for {10.2} extension twinning was determined to be ~91 ± 5 MPa in the AZ80 alloy. A CRSS increase of ~33 MPa for twinning was proposed due to precipitation strengthening.

(3) Upon tension following compression, the deformation relied on detwinning (DT1) rather than extension twinning (T2). The extension twinning mode (T2) only occurred in the first 2 cycles upon reverse tension, presumably because the higher degree of the detwinning process (DT1) in the following cycles relieved the shear stress field of {00.2} grains so that the CRSS for extension twinning was not reached.

(4) The lattice strains evolved nonlinearly during unloading and reloading, revealing that load redistributions continuously occur between "soft" and "hard" grain orientations, related to the deformation mode. The load sharing effect of the strengthening precipitates was observed that the elastically deformed precipitates tend to convey more loads during plastic deformation.

(5) Both the elevated dislocation activities and the weak particle-matrix interface contributed to the reduced LCF lifetime of this material when compared to other Mg alloys.

## Data availability

Research data in this work are available by sending direct requests to the corresponding author.

## CRediT authorship contribution statement

**Di Xie:** Writing - original draft. **Zongyang Lyu:** Writing - original draft. **Yuan Li:** Writing - original draft. **Peter K. Liaw:** Writing - original draft. **Huck Beng Chew:** Writing - original draft. **Yang Ren:** Writing - original draft. **Yan Chen:** Writing - original draft. **Ke An:** Writing - original draft. **Yanfei Gao:** Writing - original draft, All authors have contributed to the entire research process, including project design, experiments, model development, and manuscript preparation.

## Declaration of competing interest

The authors declare that they have no known competing financial interests or personal relationships that could have appeared to influence the work reported in this paper.

## Acknowledgments

This work is supported by the US National Science Foundation (DMR 1809640 to the University of Tennessee & DMR 1809696 to the University of Illinois). DX also acknowledges a graduate fellowship from Center for Materials Processing at the University of Tennessee. Neutron diffraction work was carried out at the Spallation Neutron Source (SNS), which is the U.S. Department of Energy (DOE) user facility at the Oak Ridge National Laboratory, sponsored by the Scientific User Facilities Division, Office of Basic Energy Sciences. The authors thank Dr. M. J. Frost at SNS for the technique support. This research used resources of the Advanced Photon Source, a U.S. Department of Energy (DOE) Office of Science User Facility operated for the DOE Office of Science by Argonne National Laboratory under Contract No. DE-AC02-06CH11357.

## Appendix

The Schmid factors can be calculated by $m = cos\lambda cos\phi$ with λ and φ being the angles between the loading directions and the slip (or twinning) plane normal and slip (or twinning) direction, respectively [49,50]. For a specific deformation system, i.e., {hkil}<uvtw>, the slip or twinning plane normal is reassigned by Refs. [49,50]:

$$[h_1, k_1, i_1, l_1] = \left[h, k, i, \frac{3}{2} l \left(\frac{a}{c}\right)^2\right] \qquad \text{A(1)}$$

where a and c are the lattice constants, given the c/a axial ratio as 1.624. The cosine functions, $\cos\lambda$ and $\cos\phi$, can be calculated by:

$$cos\phi(\lambda) = \frac{u_1u_2 + v_1v_2 + \frac{1}{2}(u_1v_2 + u_2v_1) + \frac{1}{3}\omega_1\omega_2\left(\frac{c}{a}\right)^2}{\sqrt{u_1^2 + v_1^2 + u_1v_1 + \frac{1}{3}\omega_1^2\left(\frac{c}{a}\right)^2} \times \sqrt{u_2^2 + v_2^2 + u_2v_2 + \frac{1}{3}\omega_2^2\left(\frac{c}{a}\right)^2}} \qquad \text{A(2)}$$

where $[u_1, v_1, t_1, w_1]$ is the new slip (twinning) plane normal or slip (twinning) direction, while $[u_2, v_2, t_2, w_2]$ is the loading direction. For a specific grain orientation, {hkil}, the loading direction $[u_2, v_2, t_2, w_2]$ can be given as $\left[h, k, i, \frac{3}{2}l\left(\frac{a}{c}\right)^2\right]$ by applying Eq. A(1).

## References

[1] A.A. Luo, Recent magnesium alloy development for elevated temperature applications, Int. Mater. Rev. 49 (1) (2004) 13–30.

[2] S. Schumann, H. Friedrich, Current and future use of magnesium in the automobile industry, Mater. Sci. Forum 419 (2003) 51–56.

[3] I.J. Polmear, Magnesium alloys and applications, Mater. Sci. Technol. 10 (1) (1994) 1–16.

[4] L. Wu, S.R. Agnew, D.W. Brown, G.M. Stoica, B. Clausen, A. Jain, D.E. Fielden, P. K. Liaw, Internal stress relaxation and load redistribution during the twinning–detwinning-dominated cyclic deformation of a wrought magnesium alloy, ZK60A, Acta Mater. 56 (14) (2008) 3699–3707.

[5] B. Clausen, C.N. Tomé, D.W. Brown, S.R. Agnew, Reorientation and stress relaxation due to twinning: modeling and experimental characterization for Mg, Acta Mater. 56 (11) (2008) 2456–2468.

[6] W. Wu, P.K. Liaw, K. An, Unraveling cyclic deformation mechanisms of a rolled magnesium alloy using in situ neutron diffraction, Acta Mater. 85 (2015) 343–353.

[7] G.E. Mann, T. Sumitomo, C.H. Cáceres, J.R. Griffiths, Reversible plastic strain during cyclic loading–unloading of Mg and Mg–Zn alloys, Mater. Sci. Eng., A 456 (1–2) (2007) 138–146.

[8] S.R. Agnew, Ö. Duygulu, Plastic anisotropy and the role of non-basal slip in magnesium alloy AZ31B, Int. J. Plast. 21 (6) (2005) 1161–1193.

[9] X. Lou, M. Li, R. Boger, S. Agnew, R. Wagoner, Hardening evolution of AZ31B Mg sheet, Int. J. Plast. 23 (1) (2007) 44–86.

[10] M.R. Barnett, M.D. Nave, C.J. Bettles, Deformation microstructures and textures of some cold rolled Mg alloys, Mater. Sci. Eng., A 386 (1–2) (2004) 205–211.

[11] L. Jiang, J.J. Jonas, R.K. Mishra, A.A. Luo, A.K. Sachdev, S. Godet, Twinning and texture development in two Mg alloys subjected to loading along three different strain paths, Acta Mater. 55 (11) (2007) 3899–3910.

[12] X.S. Wang, F. Liang, J.H. Fan, F.H. Zhang, Low-cycle fatigue small crack initiation and propagation behaviour of cast magnesium alloys based on in-situ SEM observations, Philos. Mag. A 86 (11) (2006) 1581–1596.

[13] C. Antion, P. Donnadieu, F. Perrard, A. Deschamps, C. Tassin, A. Pisch, Hardening precipitation in a Mg–4Y–3RE alloy, Acta Mater. 51 (18) (2003) 5335–5348.

[14] W. Wu, H. Qiao, K. An, X. Guo, P. Wu, P.K. Liaw, Investigation of deformation dynamics in a wrought magnesium alloy, Int. J. Plast. 62 (2014) 105–120.

[15] L. Wu, A. Jain, D.W. Brown, G.M. Stoica, S.R. Agnew, B. Clausen, D.E. Fielden, P. K. Liaw, Twinning–detwinning behavior during the strain-controlled low-cycle fatigue testing of a wrought magnesium alloy, ZK60A, Acta Mater. 56 (4) (2008) 688–695.

[16] S.R. Agnew, R.P. Mulay, F.J. Polesak, C.A. Calhoun, J.J. Bhattacharyya, B. Clausen, In situ neutron diffraction and polycrystal plasticity modeling of a Mg–Y–Nd–Zr alloy: effects of precipitation on individual deformation mechanisms, Acta Mater. 61 (10) (2013) 3769–3780.

[17] J.F. Nie, Effects of precipitate shape and orientation on dispersion strengthening in magnesium alloys, Scripta Mater. 48 (8) (2003) 1009–1015.

[18] J.D. Robson, N. Stanford, M.R. Barnett, Effect of precipitate shape and habit on mechanical asymmetry in magnesium alloys, Metall. Mater. Trans. 44 (7) (2012) 2984–2995.

[19] J.D. Robson, N. Stanford, M.R. Barnett, Effect of precipitate shape on slip and twinning in magnesium alloys, Acta Mater. 59 (5) (2011) 1945–1956.

[20] J.D. Robson, M.R. Barnett, The effect of precipitates on twinning in magnesium alloys, Adv. Eng. Mater. 21 (4) (2019) 1800460.

[21] M.R. Barnett, H. Wang, T. Guo, An Orowan precipitate strengthening equation for mechanical twinning in Mg, Int. J. Plast. 112 (2019) 108–122.

[22] W. Reimers, A.R. Pyzalla, A. Schreyer, H. Clemens, Neutrons and Synchrotron Radiation in Engineering Materials Science. From Fundamentals to Material and Component Characterization, KGaA, Wiley-VCH Verlag GmbH & Co, Weinhein, 2008.

[23] P. Staron, A. Schreyer, H. Clemens, S. Mayer, Neutrons and Synchrotron Radiation in Engineering Materials Science: from Fundamentals to Applications, John Wiley & Sons, 2017.

[24] D. Duly, M.C. Cheynet, Y. Brechet, Morphology and chemical nanoanalysis of discontinuous precipitation in Mg-Al alloys—I. Regular growth, Acta Metall. Mater. 42 (11) (1994) 3843–3854.

[25] Y. Li, C. Tan, X. Yu, Z. Nie, X. Zhao, J. Han, S. Yuan, M. Zhao, C. Guo, F. Wang, Evolution of β Mg17Al12 in MgAlZnAg alloy over time, Mater. Sci. Eng., A 754 (2019) 470–478.

[26] K. An, H.D. Skorpenske, A.D. Stoica, D. Ma, X.-L. Wang, E. Cakmak, First in situ lattice strains measurements under load at VULCAN, Metall. Mater. Trans. 42 (1) (2010) 95–99.

[27] K. An, Y. Chen, A.D. Stoica, Vulcan, A “hammer” for high-temperature materials research, MRS Bull. 44 (11) (2019) 878–885.

[28] K. An, VDRIVE-data Reduction and Interactive Visualization Software for Event Mode Neutron Diffraction. ORNL Report No. ORNL-TM-2012-621, 2012.

[29] W. Wu, S.Y. Lee, A.M. Paradowska, Y. Gao, P.K. Liaw, Twinning–detwinning behavior during fatigue-crack propagation in a wrought magnesium alloy AZ31B, Mater. Sci. Eng., A 556 (2012) 278–286.

[30] O. Muránsky, D.G. Carr, M.R. Barnett, E.C. Oliver, P. Šittner, Investigation of deformation mechanisms involved in the plasticity of AZ31 Mg alloy: in situ neutron diffraction and EPSC modelling, Mater. Sci. Eng., A 496 (1–2) (2008) 14–24.

[31] S.Y. Lee, H. Wang, M.A. Gharghouri, G. Nayyeri, W. Woo, E. Shin, P.D. Wu, W. J. Poole, W. Wu, K. An, Deformation behavior of solid-solution-strengthened Mg–9 wt.% Al alloy: in situ neutron diffraction and elastic–viscoplastic self-consistent modeling, Acta Mater. 73 (2014) 139–148.

[32] S. Agnew, D. Brown, C. Tome, Validating a polycrystal model for the elastoplastic response of magnesium alloy AZ31 using in situ neutron diffraction, Acta Mater. 54 (18) (2006) 4841–4852.

[33] S.R. Kada, P.A. Lynch, J.A. Kimpton, M.R. Barnett, In-situ X-ray diffraction studies of slip and twinning in the presence of precipitates in AZ91 alloy, Acta Mater. 119 (2016) 145–156.

[34] A. Vinogradov, E. Vasilev, M. Linderov, D. Merson, In situ observations of the kinetics of twinning–detwinning and dislocation slip in magnesium, Mater. Sci. Eng., A 676 (2016) 351–360.

[35] O. Muránsky, D.G. Carr, P. Šittner, E.C. Oliver, In situ neutron diffraction investigation of deformation twinning and pseudoelastic-like behaviour of extruded AZ31 magnesium alloy, Int. J. Plast. 25 (6) (2009) 1107–1127.

[36] H. Qiao, S.R. Agnew, P.D. Wu, Modeling twinning and detwinning behavior of Mg alloy ZK60A during monotonic and cyclic loading, Int. J. Plast. 65 (2015) 61–84.

[37] D.W. Brown, S.R. Agnew, M.A.M. Bourke, T.M. Holden, S.C. Vogel, C.N. Tomé, Internal strain and texture evolution during deformation twinning in magnesium, Mater. Sci. Eng., A 399 (1–2) (2005) 1–12.

[38] C.H. Cáceres, T. Sumitomo, M. Veidt, Pseudoelastic behavior of cast magnesium AZ91 alloy under cylic loading-unloading, Acta Mater. 51 (20) (2003) 6211–6218.

[39] Dr Drozdenko, J. Bohlen, S. Yi, P. Minárik, F. Chmelík, P. Dobroň, Investigating a twinning-detwinning process in wrought Mg alloys by the acoustic emission technique, Acta Mater. 110 (2016) 103–113.

[40] M.A. Gharghouri, G.C. Weatherly, J.D. Embury, J. Root, Study of the mechanical properties of Mg-7.7at.% Al by in-situneutron diffraction, Philos. Mag. A 79 (7) (1999) 1671–1695.

[41] C. Lv, T. Liu, D. Liu, S. Jiang, W. Zeng, Effect of heat treatment on tension–compression yield asymmetry of AZ80 magnesium alloy, Mater. Des. 33 (2012) 529–533.

[42] N. Stanford, J. Geng, Y.B. Chun, C.H.J. Davies, J.F. Nie, M.R. Barnett, Effect of plate-shaped particle distributions on the deformation behaviour of magnesium alloy AZ91 in tension and compression, Acta Mater. 60 (1) (2012) 218–228.

[43] M.A. Gharghouri, G.C. Weatherly, J.D. Embury, The interaction of twins and precipitates in a Mg-7.7 at, % Al alloy 78 (5) (1998) 1137–1149.

[44] J.J. Bhattacharyya, S.R. Kada, M.R. Barnett, S.R. Agnew, Crystal plasticity and in-situ diffraction-based determination of the dislocation strengthening and load-sharing effects of precipitates in Mg alloy, AZ91, Materialia 6 (2019).

[45] S. Ghorbanpour, B.A. McWilliams, M. Knezevic, Low-cycle fatigue behavior of rolled WE43-T5 magnesium alloy, Fatig. Fract. Eng. Mater. Struct. 42 (6) (2019) 1357–1372.

[46] S.L. Wong, P.R. Dawson, Influence of directional strength-to-stiffness on the elastic–plastic transition of fcc polycrystals under uniaxial tensile loading, Acta Mater. 58 (5) (2010) 1658–1678.

[47] L.L. Zheng, Y.F. Gao, Y.D. Wang, A.D. Stoica, K. An, X.L. Wang, Grain orientation dependence of lattice strains and intergranular damage rates in polycrystals under cyclic loading, Scripta Mater. 68 (5) (2013) 265–268.

[48] D. Catoor, Y.F. Gao, J. Geng, M.J.N.V. Prasad, E.G. Herbert, K.S. Kumar, G. M. Pharr, E.P. George, Incipient plasticity and deformation mechanisms in single-

crystal Mg during spherical nanoindentation, Acta Mater. 61 (8) (2013) 2953–2965.

[49] X.-L. Nan, H.-Y. Wang, L. Zhang, J.-B. Li, Q.-C. Jiang, Calculation of Schmid factors in magnesium: analysis of deformation behaviors, Scripta Mater. 67 (5) (2012) 443–446.

[50] J. Kwon, M.C. Brandes, P. Sudharshan Phani, A.P. Pilchak, Y.F. Gao, E.P. George, G.M. Pharr, M.J. Mills, Characterization of deformation anisotropies in an α-Ti alloy by nanoindentation and electron microscopy, Acta Mater. 61 (13) (2013) 4743–4756.